A numerical and theoretical study on viscoelastic fluid slip flows

L. L. Ferrás, A. M. Afonso, J. M. Nóbrega, and F. T. Pinho

Citation: Physics of Fluids **29**, 053102 (2017); doi: 10.1063/1.4983062
View online: http://dx.doi.org/10.1063/1.4983062
View Table of Contents: http://aip.scitation.org/toc/phf/29/5
Published by the American Institute of Physics

A numerical and theoretical study on viscoelastic fluid slip flows

L. L. Ferrás,[1,a)] A. M. Afonso,[2,b)] J. M. Nóbrega,[1,c)] and F. T. Pinho[2,d)]
[1]*Institute for Polymers and Composites/I3N, University of Minho, Campus de Azurém 4800-058 Guimarães, Portugal*
[2]*Departamento de Engenharia Mecânica, Centro de Estudos de Fenómenos de Transporte, Faculdade de Engenharia da Universidade do Porto, Rua Dr. Roberto Frias s/n, 4200-465 Porto, Portugal*

(Received 22 March 2017; accepted 21 April 2017; published online 18 May 2017)

This work describes a theoretical and numerical investigation of viscoelastic fluid flows, considering slip boundary conditions. The viscoelastic fluid is described by the simplified Phan-Thien-Tanner model, and the governing equations with slip boundary conditions are solved by a finite volume method using (1) a recently proposed methodology to control the growth of the slip velocity along the iterative process (named the SIMPLE-slip method) where some simplifications are assumed at the wall, and also (2) a slip formulation where the complete stress tensor at the wall is taken into account. Analytical and semi-analytical solutions are also provided for the fully developed flow between parallel plates of viscoelastic fluids, assuming Thomson and Troian and Lau and Schowalter non-linear wall slip models. For verification purposes, the numerical results were compared with the analytical solution for fully developed slip-flow in a planar channel using two non-linear slip models. Simulations were carried out in a classical benchmark problem in computational rheology, the viscoelastic fluid flow in a slip-stick geometry, aiming to identify the influence of slip intensity on the flow patterns, velocity, and stress growth at the singularity region. *Published by AIP Publishing.* [http://dx.doi.org/10.1063/1.4983062]

NOMENCLATURE

Symbols

c_i, $i = 1, 2, 3$	parameters of the Lau and Schowalter (LS) slip model
E	activation energy
$E_i(z)$	exponential integral
$f(tr\boldsymbol{\tau})$	scalar function of the trace of the polymer extra stress tensor
H	half channel width/thickness
k_{nl}	parameter of the nonlinear Navier slip (NNS) and LS models
m	slip exponent
$\mathbf{n}$	normal vector
p_x	streamwise pressure gradient
p	pressure
R	universal gas constant
Re	Reynolds number
t	time
T	absolute temperature
$\mathbf{u}$	velocity vector
$\mathbf{u_t}$	tangent velocity vector
$\mathbf{u_n}$	normal velocity vector
u	streamwise velocity component
v	transverse velocity component
$\mathbf{u}_{ws}$	wall slip velocity vector
U	mean velocity
Wi	Weissenberg number
x	streamwise coordinate
y	transverse coordinate

Greek Symbols

α	parameter of the Thompson and Troian (TT) slip model
β	viscosity ratio $\eta_s/(\eta_s + \eta_p)$
δn	distance from the wall to the nearest cell centre
$\dot{\gamma}$	shear rate
ε	parameter of the PTT model
η_p	polymer viscosity coefficient
η_s	solvent viscosity
λ	relaxation time of the fluid
$\mu(\dot{\gamma})$	viscosity as a function of shear rate
ρ	fluid density
$\boldsymbol{\tau}$	polymeric extra-stress tensor
$\boldsymbol{\tau_t}$	tangent polymeric extra-stress tensor
τ_{xy}	shear stress
τ_{xx}	normal stress
τ_{yy}	normal stress

I. INTRODUCTION

Wall slip is a relevant phenomenon in many engineering processes, especially those involving high molecular weight macromolecules, as occurs, for example, in polymer processing as described in a variety of experiments reported in the literature.[1,2] Among others, fluids that exhibit wall slip are the polyvinyl chloride (PVC), high-density polyethylene, elastomers, suspensions, and some food products.[3]

Given the complexity of the constitutive equations required to represent the rheological behavior of viscoelastic fluids, and also the effects of wall slip, computational simulations of this type of fluid flows require the use of robust numerical methods. To handle these problems, a new method

a)Electronic mail: luis.ferras@dep.uminho.pt.
b)Electronic mail: aafonso@fe.up.pt
c)Electronic mail: mnobrega@dep.uminho.pt
d)Electronic mail: fpinho@fe.up.pt

was recently developed to solve the pressure equation and to control the growth of the slip velocity throughout the iterative process, named the SIMPLE-slip method,[4] which was implemented in an in-house computational rheology code[5] and used here to predict numerically the slip-stick flow of a simplified Phan-Thien-Tanner (sPTT) fluid[6,7] together with the linear and nonlinear Navier slip boundary conditions.[8] The SIMPLE-slip method was used with nonlinear slip boundary conditions such as the nonlinear Navier,[8] the Hatzikiriakos,[9] and asymptotic slip models,[10] and presented better numerical convergence for higher values of the Weissenberg number and of the slip coefficient, than the classic explicit implementation of wall slip,[4] but it also invoked some simplifying assumptions, which we show in this work to provide accurate results by comparing it with a method relying on the full stress tensor at the wall.

As referred above, the two methods (SIMPLE-slip and full stress tensor at the wall) are compared. The results obtained show that the full stress tensor at the wall gives rise to convergence difficulties, mainly due to the decoupling between the stress and velocity variables in the vicinity of the wall, but, no simplifications are assumed for the stress at the wall, as was the case of the SIMPLE-slip method.

In this work, we also further extend the use of the SIMPLE-slip method by implementing it together with the slip models given by Thomson and Troian (TT)[11] (a model that is controlled by the extent to which the liquid feels corrugations and relates the degree of slip to the underlying static properties and dynamic interactions between wall and fluid) and by Lau and Schowalter (LS)[12] (a slip model that was derived by applying the concept of junctions between the wall and fluid interfaces and that depends on the shear stress and the temperature), and we also present a detailed study of the slip-stick flow under partial wall slip boundary conditions.

Additionally, in the analytical study, we present closed form solutions for the LS[12] model after invoking some simplifications. For the cases where an analytical solution was not obtained with the TT[11] and LS[12] models, we prove the existence of unique solutions and provide the range where they lie, thus facilitating the task of finding solutions using a semi-analytical methodology.

The Introduction is followed by Section II, where the relevant governing equations are presented. In Section III, we present the analytical solution for the fully developed slip-flow of polymer solutions described by the sPTT or finitely-extensive-nonlinear-elastic with Peterlin's closure (FENE-P)[13] models in a planar channel for the TT and LS nonlinear slip models, which is used for verification purposes. In Section IV, we briefly describe the numerical method used to solve and couple the Navier-Stokes equations together with the nonlinear Navier slip boundary condition and present a suitable linearization for the TT and LS wall slip velocity models. In Section V, the results obtained from the simulations of an sPTT fluid on a slip-stick geometry are discussed and the paper ends with the conclusions in Section VI.

II. GOVERNING EQUATIONS

The governing equations for isothermal incompressible fluid flow are the mass conservation equation

$$\nabla \cdot \mathbf{u} = 0 \tag{1}$$

and the linear momentum conservation equation

$$\rho\left(\frac{\partial \mathbf{u}}{\partial t} + \nabla \cdot \mathbf{uu}\right) = -\nabla p + \nabla \cdot \boldsymbol{\tau} + \eta_s \nabla^2 \mathbf{u}, \tag{2}$$

where $\mathbf{u}$ is the velocity vector, p is the pressure, ρ is the fluid density, η_s is the solvent viscosity, and $\boldsymbol{\tau}$ is the extra stress tensor for the polymer, which is given by the following differential constitutive equation, called the simplified Phan-Thien-Tanner model (sPTT):[6,7]

$$f(tr\boldsymbol{\tau})\boldsymbol{\tau} + \lambda\left(\frac{\partial \boldsymbol{\tau}}{\partial t} + \mathbf{u}\cdot\nabla\boldsymbol{\tau} - (\nabla\mathbf{u})^T\cdot\boldsymbol{\tau} - \boldsymbol{\tau}\cdot\nabla\mathbf{u}\right) = \eta_p\left(\nabla\mathbf{u} + (\nabla\mathbf{u})^T\right). \tag{3}$$

In Eq. (3), $f(tr\boldsymbol{\tau})$ is a function of the trace of the extra stress tensor, λ is the relaxation time, and η_p is the zero-shear polymer viscosity. There are two possible functions for $f(tr\boldsymbol{\tau})$ in the sPTT model, but only the original linear function[6] is considered here

$$f(tr\boldsymbol{\tau}) = 1 + \frac{\varepsilon\lambda}{\eta_p} tr(\boldsymbol{\tau}) \tag{4}$$

with ε representing the extensibility parameter that primarily influences the elongational behavior of the fluid.

When considering slip boundary conditions at the wall, the usual Dirichlet velocity boundary condition $\mathbf{u} = \mathbf{0}$ is substituted by the nonlinear Navier slip (NNS) model[8]

$$\|\mathbf{u}_{ws}\| = k_{nl}\|\boldsymbol{\tau}_w\|^m, \quad m > 0, \tag{5}$$

where $\mathbf{u}_{ws}$ is the slip velocity vector (ws stands for wall slip), $\boldsymbol{\tau}_w$ is the tangent stress vector, k_{nl} is the slip coefficient that allows controlling the amount of slip, m is the slip exponent that gives the model its nonlinearity (k_{nl} and m are both model parameters), and $\|.\|$ is the usual l^2-norm operator.

The wall slip TT model[11] is given by

$$\|\mathbf{u}_{ws}\| = \alpha\left(1 - \frac{\|\boldsymbol{\tau}_w\|}{\|\boldsymbol{\tau}_w\|_c}\right)^{-1/2}\|\boldsymbol{\tau}_w\|, \tag{6}$$

where $\|\boldsymbol{\tau}_w\|_c$ is some critical (maximum) tangent stress (its value is such that $1 - \|\boldsymbol{\tau}_w\|/\|\boldsymbol{\tau}_w\|_c \geq 0$ is always observed) and α is a model parameter. Following the notation of Ref. 14, Eq. (6) can be rewritten as

$$\|\mathbf{u}_{ws}\| = \alpha(1 - \beta\|\boldsymbol{\tau}_w\|)^{-1/2}\|\boldsymbol{\tau}_w\| \tag{7}$$

with $\beta \equiv \|\boldsymbol{\tau}_w\|_c^{-1}$ and $\alpha,\ \beta > 0$.

The LS slip velocity model[12] is given by

$$\|\mathbf{u}_{ws}\| = c_1\|\boldsymbol{\tau}_w\|^m\left[1 - c_2\tanh\left(\frac{E - c_3\|\boldsymbol{\tau}_w\|}{RT}\right)\right], \tag{8}$$

where c_1, c_2, and c_3 are the empirical coefficients, E is the activation energy, R is the universal gas constant, and T is the absolute temperature.

III. ANALYTICAL SOLUTIONS

Assuming a fully developed Poiseuille flow and some simplifications in the slip models, it is possible to obtain a closed form analytical solution for the inverse problem with the LS slip model.

After an adequate normalization of the governing equations and the slip velocity law (for details, see Appendix A) and considering that $m = 1$ and $\frac{E+c_3'(p_x')}{RT} \ll 1$ then $\tanh\left(\frac{E+c_3'(p_x')}{RT}\right) \approx \frac{E+c_3'(p_x')}{RT}$. Under these assumptions, and imposing a specific flow rate, the solution is given by (see details in Appendix A)

$$u'\left(y'\right) = 0.5p_x'\left(y'^2-1\right) + 0.5\varepsilon Wi^2 p_x'^3\left(y'^4-1\right) + c_1'\left(-p_x'\right)\left[1-c_2\left(\frac{E+c_3'\left(p_x'\right)}{RT}\right)\right] \tag{9}$$

with

$$p_x' = \sqrt[3]{-\frac{P}{2}+\sqrt{\frac{P^2}{4}+\frac{S^3}{27}}} + \sqrt[3]{-\frac{P}{2}-\sqrt{\frac{P^2}{4}+\frac{S^3}{27}}} - \frac{a_1}{3} \tag{10}$$

and

$$\begin{aligned} a_1 &= -\frac{5c_1'c_2c_3'}{2RT}, \\ a_2 &= \frac{-\frac{1}{3}-c_1'+\frac{c_1'c_2E}{RT}}{-\frac{2}{5}\varepsilon Wi^2}, \\ a_3 &= \left(\frac{2}{5}\varepsilon Wi^2\right)^{-1}, \\ P &= a_3 - \frac{a_1a_2}{3} + \frac{2a_1^3}{27}, \\ S &= a_2 - \frac{a_1^2}{3}, \end{aligned} \tag{11}$$

where length, velocity, and stresses were scaled with H, U, and $\eta U/H$, respectively, U is the mean streamwise velocity, H is the half channel width, and $Wi = \lambda U/H$ is the Weissenberg number.

For an higher order truncated Taylor series expansion, $\tanh\left(\frac{E+c_3'(p_x')}{RT}\right) \approx \frac{E+c_3'(p_x')}{RT} - \frac{1}{3}\left(\frac{E+c_3'(p_x')}{RT}\right)^3$, a closed form solution is still possible because the equation to solve for p_x' is quartic

$$\begin{aligned} &\left(-\frac{c_1'c_2c_3'^3}{3(RT)^3}\right)p_x'^4 + \left(\frac{c_1'c_2c_3'^2E}{3(RT)^3} - \frac{2}{5}\varepsilon Wi^2\right)p_x'^3 \\ &+\left(\frac{c_1'c_2c_3'}{RT} + \frac{c_1'c_2c_3'E^2}{3(RT)^3}\right)p_x'^2 \\ &+\left(-\frac{1}{3} - c_1' + \frac{c_1'c_2E}{RT} - \frac{c_1'c_2E^3}{3(RT)^3}\right)p_x' - 1 = 0 \end{aligned} \tag{12}$$

and the procedure to solve this equation for p_x' can be found in many algebra books (e.g., Ref. 15).

As shown in Appendix A, for the other slip models, it is still possible to obtain semi-analytic solutions.

IV. NUMERICAL METHOD

A. SIMPLE-slip

The in-house code used is a three-dimensional time dependent finite-volume method (FVM),[5] with subsequent improvements described in Refs. 16–19. The FVM code uses collocated non-orthogonal structured meshes, central differences for the discretization of diffusive terms, the CUBISTA scheme[19] for the advective terms, with third-order accuracy in uniform meshes, and a second-order backward implicit time discretization through the SIMPLEC algorithm[20] to ensure simultaneously the momentum balance and mass conservation. The Rhie and Chow interpolation method[21] is used to couple the pressure and velocity fields in a collocated mesh arrangement as described in detail in Ref. 22.

The main modifications required to implement the slip boundary conditions are briefly explained. To illustrate the implementation of slip, we assume that the equations are solved in a simple 2D Poiseuille flow with Cartesian coordinates and orthogonal meshes (cf. Fig 1). Since the slip velocity vector is tangent to the wall (Fig. 2), the x−component of the tangent stress vector $\boldsymbol{\tau}_t$ is determined by the projection of $\boldsymbol{\tau}_t$ in the x−direction.

For the SIMPLE-slip method,[4] we assume a Couette flow in the vicinity of the wall, and the shear stress at the upper wall is given by

$$\tau_t = \mu(\dot{\gamma})\left.\frac{\mathrm{d}u}{\mathrm{d}y}\right|_{wall} \tag{13}$$

with the viscosity function $\mu(\dot{\gamma})$ depending on the constitutive model used. For the sPTT fluid model, $\mu(\dot{\gamma})_{wall} \equiv \eta_s + \frac{\eta_p}{1+(\alpha-1)^2/3\alpha}$, with $\alpha \equiv \left(\theta+\sqrt{\theta^2-1}\right)^{1/3}$ and $\theta \equiv 1 + 27\varepsilon(\lambda\dot{\gamma})^2_{wall}$.[23] Under these flow conditions, the nonlinear Navier slip model takes the form

$$u_{ws} = \mathrm{f_{wall}}\left(\frac{du}{dy}\right)k_{nl}\left|\mu(\dot{\gamma})\frac{du}{dy}\right|^m_{wall}, \tag{14}$$

where the function $\mathrm{f_{wall}}$ is given by

$$\mathrm{f_{wall}} = \begin{cases} -1 & \text{top wall} \\ +1 & \text{bottom wall} \end{cases}. \tag{15}$$

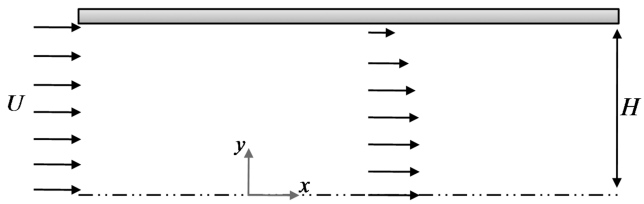

FIG. 1. Schematic representation of the channel flow geometry.

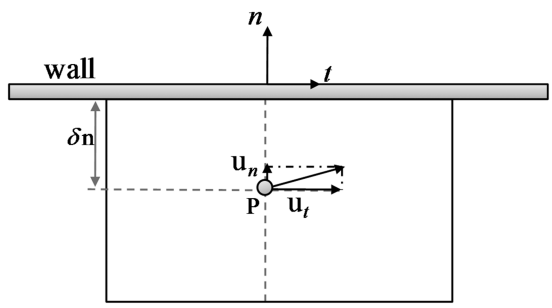

FIG. 2. Projection of the velocity vector at the center of the computational cell into its tangent and normal components (left—orthogonal mesh; right—non-orthogonal mesh).

The continuity and momentum equations can be written in Cartesian coordinates as Eqs. (16) and (17), respectively,

$$\frac{\partial u}{\partial x}+\frac{\partial v}{\partial y}=0, \tag{16}$$

$$\rho\left[\frac{\partial \phi}{\partial t}+\frac{\partial (u\phi)}{\partial x}+\frac{\partial (v\phi)}{\partial y}\right]=-\frac{\partial p}{\partial \Psi}+\frac{\partial}{\partial x}\left(\eta_s\frac{\partial \phi}{\partial x}+\tau_{\Psi x}\right)+\frac{\partial}{\partial y}\left(\eta_s\frac{\partial \phi}{\partial y}+\tau_{\Psi y}\right), \tag{17}$$

where $\phi = u$, $\Psi = x$ in the x-momentum equation, and $\phi = v$, $\Psi = y$ in the y-momentum equation. The discretization of the continuity equation in a computational cell P (Fig. 2) results in the balance of mass fluxes for this cell. These fluxes are normal to the cell faces and therefore, the slip boundary condition has no direct influence on this discretized equation (since the walls are impermeable). On the other hand, the discretized form of the integrated momentum equation is directly affected by the slip boundary condition, and for that reason, its discretization is briefly explained below. The interested reader should consult Refs. 16 and 17 for further details.

In the vicinity of the wall, only the diffusive term is affected by the slip velocity. For the sPTT fluid, the discretization of this term together with the assumption of Eq. (13) leads to the following expression:

$$\left[\left(\mu(\dot\gamma)\frac{\partial \phi}{\partial y}\right)_{n\equiv wall}-\left(\eta_s\frac{\partial \phi}{\partial y}+\tau_{\Psi y}\right)_s\right]\Delta x\Delta t+\left[\left(\eta_s\frac{\partial \phi}{\partial x}+\tau_{\Psi x}\right)_e-\left(\eta_s\frac{\partial \phi}{\partial y}+\tau_{\Psi x}\right)_w\right]\Delta y\Delta t, \tag{18}$$

where the subscripts n, s, e, and w stand for north, south, east, and west faces, respectively, and Δx, Δy, and Δt are the mesh sizes and time step, respectively.

Note that the single term for the north cell face $(\ldots)_n$ in Eq. (18) arises from Eq. (13) (the north cell face is a wall boundary face) and incorporates both the solvent and polymer contributions via a total viscosity function $\mu(\dot\gamma)_{wall}$. The slip velocity is then introduced via the term $\left(\frac{\partial \phi}{\partial y}\right)_{n\equiv wall}$. For ease of understanding, assume the one-sided approximation to the derivatives, such as the first order scheme of Eq. (19),

$$\left(\frac{\partial \phi}{\partial y}\right)_{wall}=\frac{\phi_{wall}-\phi_{\mathrm{P}}}{\Delta y_f}+O(\triangle y) \tag{19}$$

(Δy_f stands for half cell width) together with uniform orthogonal meshes and central differences to discretize all diffusion-related derivatives (except at the boundaries). Then, the first term in Eq. (18) becomes

$$\left[\frac{\mu(\dot\gamma)_{wall}}{\Delta y_f}\phi_n+\frac{\eta_s}{\Delta y}\phi_{\mathrm{S}}-\left(\frac{\mu(\dot\gamma)_{wall}}{\Delta y_f}+\frac{\eta_s}{\Delta y}\right)\phi_{\mathrm{P}}-\left(\tau_{\Psi y}\right)_s\right]\Delta x\Delta t. \tag{20}$$

After grouping this term with all the other terms, the final form of the discretized momentum equation is rewritten in the standard compact form (in which, we have substituted the general variable ϕ by the specific variable u since we are analyzing the x-momentum equation)

$$a_{\mathrm{P}}u_{\mathrm{P}}=a_{\mathrm{E}}u_{\mathrm{E}}+a_{\mathrm{W}}u_{\mathrm{W}}+a_{\mathrm{S}}u_{\mathrm{S}}+\underbrace{a_{\mathrm{N}}u_{\mathrm{N}}+\frac{\Delta V_{\mathrm{P}}\,(\rho u)^0_{\mathrm{P}}}{\Delta t}+\frac{\delta p}{\delta x}+S_{stress}}_{source\ terms}, \tag{21}$$

where $\frac{\delta p}{\delta x}$ represents a general discretization of the pressure gradient, S_{stress} represents the stress contribution, ΔV_{P} is the volume of cell P, the superscript "0" stands for values that come from the previous iteration, and a_{E}, a_{S}, a_{W} are given by Eqs. (22)–(24), respectively,

$$a_{\mathrm{E}}=a^c_{\mathrm{E}}+a^d_{\mathrm{E}}=a^c_{\mathrm{E}}+\frac{\eta_s\Delta y}{\Delta x}, \tag{22}$$

$$a_{\mathrm{S}}=a^c_{\mathrm{S}}+a^d_{\mathrm{S}}=a^c_{\mathrm{S}}+\frac{\eta_s\Delta x}{\Delta y}, \tag{23}$$

$$a_{\mathrm{W}}=a^c_{\mathrm{W}}+a^d_{\mathrm{W}}=a^c_{\mathrm{W}}+\frac{\eta_s\Delta y}{\Delta x} \tag{24}$$

with the superscripts c and d referring to the convective and diffusive contributions, respectively. To account for the slip boundary condition, which affects $a_{\mathrm{N}}u_{\mathrm{N}} = a_{\mathrm{N}}u_{\mathrm{wall}}$, the coefficient a_{N} is given by

$$a_{\mathrm{N}}=\frac{\mu(\dot\gamma)_{wall}\Delta x}{\Delta y_f}. \tag{25}$$

Note that N stands for the north cell, which in this case refers to the boundary wall. This is why $a_{\mathrm{N}}u_{\mathrm{N}}$ is in the source term of Eq. (21).

Regarding the convective terms, since they are not affected by the slip velocity, they are handled as described in Ref. 5. Finally the central coefficient a_{P} is given as in the standard procedure[17] by

$$a_{\mathrm{P}}=a_{\mathrm{E}}+a_{\mathrm{W}}+a_{\mathrm{S}}+a_{\mathrm{N}}+\frac{\rho\Delta V_{\mathrm{P}}}{\Delta t}. \tag{26}$$

Assuming the approximation of Eq. (19), let i represent the number of the outer iteration (iteration between the linearized momentum equation and the pressure correction equation), then, the discretized slip boundary condition at iteration i is given by (see Fig. 2)

$$u^i_{ws}=k_{nl}\left(\frac{\mu(\dot\gamma)_w}{\delta n}\right)^m(u^{i-1}_{\mathrm{P}}-u^{i-1}_{ws})\left|(u^{i-1}_{ws}-u^{i-1}_{\mathrm{P}})\right|^{m-1}. \tag{27}$$

Here, at each iteration i, the boundary condition is updated with the velocity from the previous iteration, $i-1$. In order to achieve convergence, the variation of this slip velocity boundary condition along the iterative process must be bounded. Sudden changes in the boundary condition along the iterative process will be detrimental for the overall convergence. Due to this inconsistency, non-physical values may appear, and the iterative process can diverge. The relationship $|u_{ws}| < |u_{\mathrm{P}}|$ seems to be the key to the convergence of the iterative process.[4] Therefore, we linearized the previous equation assuming that u_{ws} (at the right-hand-side) is evaluated at the present iteration as happens with the left-hand-side value, i.e.,

$$u^i_{ws}=k_{nl}\left(\frac{\mu(\dot\gamma)^{i-1}_w}{\delta n}\right)^m\left(u^{i-1}_{\mathrm{P}}-u^i_{ws}\right)\left|u^{i-1}_{\mathrm{P}}-u^{i-1}_{ws}\right|^{m-1}. \tag{28}$$

The method is semi-implicit in the linearized velocity difference, and Eq. (28) can be rewritten as

$$u^i_{ws}=\frac{a}{a+1}u^{i-1}_{\mathrm{P}} \tag{29}$$

with $a = (k_{nl}\mu(\dot{\gamma})_{wall}/\delta n)^m \left|u_{\mathrm{P}}^{i-1} - u_{ws}^{i-1}\right|^{m-1}$. In this way, the absolute slip velocity $|u_{ws}|$ is always bounded by $\left|u_{\mathrm{p}}\right|$ because $0 \leq a/(a+1) < 1$.

The other two slip models can also be linearized in a similar way. For the TT slip model, this would be

$$u_{ws}^{i} = \alpha\mu\left(\delta n^2 - \delta n\beta\mu\left|u_{\mathrm{P}}^{i-1} - u_{ws}^{i-1}\right|\right)^{-1/2}\left(u_{\mathrm{P}}^{i-1} - u_{ws}^{i}\right), \quad (30)$$

which can be rewritten as

$$u_{ws}^{i} = \frac{b}{b+1}u_{\mathrm{P}}^{i-1} \quad (31)$$

with $\beta\mu|u_{\mathrm{P}}^{i-1} - u_{ws}^{i-1}| < \delta n$ and $b = \alpha(\delta n^2 - \delta n\beta\mu|u_{\mathrm{P}}^{i-1} - u_{ws}^{i-1}|)^{-1/2}$.

During the iterative procedure, and especially at the beginning, the difference $|u_{\mathrm{P}}^{i-1} - u_{ws}^{i-1}|$ can be substantial and eventually lead to $\beta\mu|u_{\mathrm{P}}^{i-1} - u_{ws}^{i-1}| \geq \delta n$, and this may result in the divergence of the computation or in float errors. To avoid this potential problem, we used classical relaxation when updating this term at each iteration.

For the LS slip model, the linearization is given by

$$u_{ws}^{i} = \frac{c_1\mu^m}{\delta n^m}\left(u_{\mathrm{P}}^{i-1} - u_{ws}^{i}\right)\left|u_{\mathrm{P}}^{i-1} - u_{ws}^{i-1}\right|^{m-1} \times\left[1 - c_2\tanh\left(\frac{E - \frac{c_3\mu}{\delta n}\left|u_{\mathrm{P}}^{i-1} - u_{ws}^{i-1}\right|}{RT}\right)\right], \quad (32)$$

which is equivalent to

$$u_{ws}^{i} = \frac{c}{c+1}u_{\mathrm{P}}^{i-1} \quad (33)$$

with $c = \frac{c_1\mu^m}{\delta n^m}\left|u_{\mathrm{P}}^{i-1} - u_{ws}^{i-1}\right|^{m-1}\left[1 - c_2\tanh\left(\frac{E - \frac{c_3\mu}{\delta n}|u_{\mathrm{P}}^{i-1} - u_{ws}^{i-1}|}{RT}\right)\right]$.

The main feature of this method is that the slip velocity is always smaller (in modulus) than the velocity at the center of the adjacent computational cell, a requirement for convergence which is also supported by physical arguments.

To solve the system of equations, we use the following iterative procedure:

1. Set the boundary conditions, the initial velocity, and pressure fields;
2. Solve the extra stress equations for the non-Newtonian model;
3. Compute the slip velocity with the semi-implicit discretized slip model, Eqs. (29) and (31) or (33);
4. Solve the linearized momentum equation;
5. Solve the pressure correction equation;
6. Correct the velocity and pressure fields;
7. Check for convergence in the residuals of the system of equations;
8. If convergence is not achieved proceed to step 2, otherwise the solution was obtained.

Providing that the mesh is orthogonal, a semi-implicit method to calculate the slip boundary condition could also be used, as described in Appendix B. The implementation of the slip boundary conditions can also be generalized for any slip velocity function, as shown in Appendix C.

1. Theoretical assessment of the validity of the wall slip Couette flow assumption

This previous method relies on the assumption that the flow in the vicinity of the wall is essentially viscometric in the presence of wall slip. Theoretically, unless the flow is fully developed, this approximation is wrong, as we will now show.

Consider the constitutive equations in two dimensions (written in Cartesian coordinates) for the steady 2D Poiseuille flow (Fig. 1). For the particular case of $\varepsilon = 0$ (Oldroyd-B model), we have the following system of equations:

$$\begin{cases} \tau_{xx} + \lambda\left(u\frac{\partial\tau_{xx}}{\partial x} + v\frac{\partial\tau_{xx}}{\partial y}\right) = 2\eta_p\frac{\partial u}{\partial x} + 2\lambda\left(\tau_{xx}\frac{\partial u}{\partial x} + \tau_{xy}\frac{\partial u}{\partial y}\right), \\ \tau_{xy} + \lambda\left(u\frac{\partial\tau_{xy}}{\partial x} + v\frac{\partial\tau_{xy}}{\partial y}\right) = \eta_p\left(\frac{\partial u}{\partial y} + \frac{\partial v}{\partial x}\right) + \lambda\left(\tau_{xx}\frac{\partial v}{\partial x} + \tau_{yy}\frac{\partial u}{\partial y}\right), \\ \tau_{yy} + \lambda\left(u\frac{\partial\tau_{yy}}{\partial x} + v\frac{\partial\tau_{yy}}{\partial y}\right) = 2\eta_p\left(\frac{\partial v}{\partial y}\right) + 2\lambda\left(\tau_{xy}\frac{\partial v}{\partial x} + \tau_{yy}\frac{\partial v}{\partial y}\right). \end{cases} \quad (34)$$

For a small layer of fluid in the vicinity of the top wall (Fig. 2), some simplifications can be performed because $v = 0$ and $\frac{\partial v}{\partial x} = 0$,

$$\begin{cases} \tau_{xx} + \lambda u\frac{\partial\tau_{xx}}{\partial x} = 2\eta_p\frac{\partial u}{\partial x} + 2\lambda\left(\tau_{xx}\frac{\partial u}{\partial x} + \tau_{xy}\frac{\partial u}{\partial y}\right), \\ \tau_{xy} + \lambda u\frac{\partial\tau_{xy}}{\partial x} = \eta_p\frac{\partial u}{\partial y} + \lambda\tau_{yy}\frac{\partial u}{\partial y}, \\ \tau_{yy} + \lambda u\frac{\partial\tau_{yy}}{\partial x} = 2\eta_p\frac{\partial v}{\partial y} + 2\lambda\tau_{yy}\frac{\partial v}{\partial y}. \end{cases} \quad (35)$$

a. Fully developed flow. For the case of a fully developed flow, we have $\frac{\partial}{\partial x} = 0$ (except for the pressure), $\frac{\partial u}{\partial y} = const$, $\frac{\partial u}{\partial x} = 0 \Rightarrow u = const$ (const = constant), and, by continuity, $\frac{\partial v}{\partial y} = 0$.

The previous system of equations is then given by

$$\begin{cases} \tau_{xx} = 2\lambda\eta_p\left(\frac{\partial u}{\partial y}\right)^2, \\ \tau_{xy} = \eta_p\frac{\partial u}{\partial y}, \\ \tau_{yy} = 0. \end{cases} \quad (36)$$

This solution is valid for both no-slip and constant slip boundary conditions and it reveals that in regions where the flow is fully developed, our approximation (Couette flow assumption in the vicinity of the wall) is correct since $\tau_{xy} = \eta_p\frac{\partial u}{\partial y}$.

b. Regions where the fluid is not fully developed. Before showing the influence of the Couette flow approximation in the vicinity of the wall by performing numerical simulation, we will first exemplify the effects of this approximation making use of a simple and particular case.

Since the fluid is allowed to slip with a varying slip velocity along the wall, then $u \neq 0$ and $\frac{\partial}{\partial x} \neq 0$, leading to the system of Eq. (35).

In order to attempt a solution for this set of equations, we need to provide the velocity profile $u(x)$ and $\frac{\partial u}{\partial y}(x)$.

Therefore, we now study the solution of this system of equations for a particular case of $Wi = \lambda U/H = 0.5$. From numerical simulations of Poiseuille flow between parallel plates at $Wi = 0.5$ (considering the full stress tensor at the wall and the Navier slip boundary condition), we observed that the slip velocity is higher at the entrance of the channel and then

decreases (following a somewhat exponential decay) along the channel until a fully developed flow is obtained. Therefore, let us assume an exponential decay function for the following theoretical analysis:

$$u(x) = c\exp(-x), \tag{37}$$

where c is a constant that allows a more general velocity profile. Note that far from the entrance, the slip velocity is very small (when compared to the high gradients in channel entrance singularity), but, the region of interest in this analysis is near the entrance of the channel where the flow is not fully developed.

From the same numerical simulations, we could also find an increase of $\frac{\partial u}{\partial y}$ (at the wall) along the channel (decrease in magnitude) with a magnitude $\approx 10^3$ higher than the slip velocity; therefore, we have considered the following expression for the velocity normal derivative at the wall:

$$\frac{\partial u}{\partial y}(x) = -10^3\left[c\exp(-x)+1\right]. \tag{38}$$

These are the functions that will be used in order to find an analytical solution for the stresses at Eq. (35).

The equation for the τ_{yy} stress component does not depend directly on the other stress components, and, it can be rewritten as

$$\tau_{yy} + a\frac{\partial \tau_{yy}}{\partial x} = b \tag{39}$$

with $a = \frac{\lambda u}{\left(1-2\lambda\frac{\partial v}{\partial y}\right)}$ and $b = \frac{2\eta_p\frac{\partial v}{\partial y}}{\left(1-2\lambda\frac{\partial v}{\partial y}\right)}$ ($\frac{\partial v}{\partial y}$ can be easily obtained from continuity and Eq. (37)).

Assuming $c = 1$ and that the boundary $\tau_{yy\,|\,x=0} = 0$ holds at the inlet boundary, the solution of Eq. (39) is given by

$$\begin{aligned}\tau_{yy}(x) = {} & \frac{\exp(-\frac{\exp(x)}{\lambda})\eta_p\lambda\left(-\exp(\frac{\exp(x)}{\lambda}+x)-\lambda\exp(\frac{\exp(x)}{\lambda})+\exp(\frac{1}{\lambda}+2x)(1+\lambda)\right)}{\lambda^3} \\ & + \frac{\exp(-\frac{\exp(x)}{\lambda}+2x)\eta_p\left(Ei\left(\frac{\exp(x)}{\lambda}\right)-Ei\left(\frac{1}{\lambda}\right)\right)}{\lambda^3},\end{aligned} \tag{40}$$

where $Ei(z)$ stands for the exponential integral

$$Ei(z) = \frac{1}{2}\left(\ln(z)-\ln\left(\frac{1}{z}\right)\right)+\sum_{m=1}^{\infty}\frac{z^m}{mm!}+\gamma, \tag{41}$$

which is a particular case of the more general hypergeometric functions, and, γ is the Euler-Mascheroni constant.

This equation can be used to find the τ_{xy} stress component (second differential equation from Eq. (35)), which is given by (assuming $\tau_{xy\,|\,x=0} = 0$)

$$\begin{aligned}\tau_{xy}(x) = {} & -\frac{500\exp(-\frac{\exp(x)}{\lambda})\eta_p\lambda\exp(\frac{\exp(x)}{\lambda})\left(-3\exp(x)-2\exp(2x)-3\lambda-2\lambda\exp(x)+2\lambda^2\right)}{3\lambda^3} \\ & - \frac{500\exp(-\frac{\exp(x)}{\lambda})\eta_p\lambda\exp(\frac{1}{\lambda})\left(3\exp(2x)+2\exp(3x)+3\lambda\exp(2x)+2\lambda\exp(3x)-2\lambda^2\right)}{3\lambda^3} \\ & - \frac{500\exp(-\frac{\exp(x)}{\lambda}+2x)(3+2\exp(x))\eta_p\left(Ei\left(\frac{\exp(x)}{\lambda}\right)-Ei\left(\frac{1}{\lambda}\right)\right)}{3\lambda^3}.\end{aligned} \tag{42}$$

By letting $x \to +\infty$, we can easily show that as we move away from the channel entrance we are no longer under the strong influence of the initial boundary conditions, and,

$$\tau_{yy}(x) \to 0, \tag{43}$$

$$\tau_{xy}(x) \to \eta_p\frac{\partial u}{\partial y}. \tag{44}$$

In this way, the fully developed solution (Eq. (36)) is recovered.

The analytical solution for τ_{xx} is also possible, after the substitution of Eqs. (40) and (42) into Eq. (35). Note that for this specific problem, only τ_{xy} and τ_{yy} are required for the momentum equation and τ_{xy} for the slip velocity model.

In Fig. 3, we can see the variation of τ_{yy} (Eq. (40)) and τ_{xy} (Eq. (42)) along the channel wall. A drastic increase (in magnitude) at the entrance of the channel occurs for both quantities, followed by an exponential decrease (in magnitude).

When we assume a Couette flow in the vicinity of the wall, τ_{xy} should be constant along the channel wall, and, from this theoretical analysis, the correct boundary condition at the entrance of the channel would be $\tau_{xy\,|\,x=0} = \eta_p\frac{\partial u}{\partial y}$. When solving the system of governing equations for the complete channel geometry, we have an evolution equation for the stresses; therefore, we can impose a null shear stress at the entrance that will result in the increase of the shear stress along the channel, until it fully develops. Therefore, we expect a similar behavior to the one obtained for the slip velocity case, shown in Fig. 3.

Although our Couette-slip approximation does not match exactly the analytical solution in regions where the flow is not fully developed, under certain assumptions, it is a good approximation (as shown later). Due to the complexity of the system of differential equations involved (especially if $\varepsilon \neq 0$), a full theoretical analysis is difficult.

This theoretical analysis is restricted to a near wall region, thus neglecting the influence of the rest of the flow

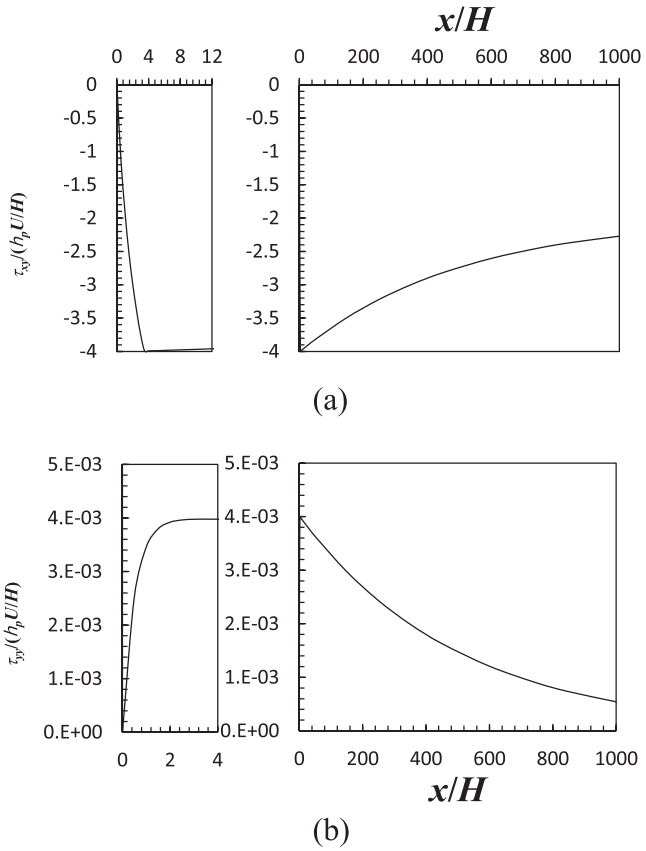

FIG. 3. Variation of the stresses (a) τ_{xy}, Eq. (42), and (b) τ_{yy}, Eq. (40), along the channel wall (left: zoomed view of the stress development near the entrance of the channel).

domain. Next the Couette flow assumption at the wall will be numerically compared with a full wall stress approximation by performing numerical simulations for the slip-stick benchmark problem.

B. Slip formulation with the complete stress vector at the wall

The slip method previously described relies on the assumption that the flow in the vicinity of the wall is essentially viscometric; now we use the complete stress tensor formulation, where the stress tensor at the wall is obtained by extrapolation from the inner cells.

1. Proposed method

Only the diffusive term of the momentum equation needs to be modified, in order to implement the slip boundary conditions. If the total stress tensor at the wall is to be considered, the discretization of Equation (17) results in the following equation:

$$\left[\left(\eta_s\frac{\partial\phi}{\partial y}+\tau_{\Psi y}\right)_{n\equiv wall}-\left(\eta_s\frac{\partial\phi}{\partial y}+\tau_{\Psi y}\right)_{s}\right]\Delta x\Delta t + \left[\left(\eta_s\frac{\partial\phi}{\partial x}+\tau_{\Psi x}\right)_{e}-\left(\eta_s\frac{\partial\phi}{\partial y}+\tau_{\Psi x}\right)_{w}\right]\Delta y\Delta t. \quad (45)$$

The terms of interest are the ones evaluated at the wall, $\eta_s\frac{\partial\phi}{\partial y}_{n\equiv wall}$ and $\tau_{\Psi y_{n\equiv wall}}$.

For the evaluation of $\eta_s\frac{\partial\phi}{\partial y}_{n\equiv wall}$, a procedure similar to that presented in the SIMPLE-slip method (see Eqs. (19)–(26)) can be used, with the constant viscosity η_s instead of $\mu(\dot\gamma)$.

In order to capture the complete stress at the wall $\left(\tau_{\Psi y_{n\equiv wall}}\right)$, we used linear extrapolation of the stresses to the wall from stresses at the adjacent inner cells, where these have been obtained from the numerical solution of the constitutive equation.

For the evaluation of the slip velocity models via any of the chosen slip models (Eqs. (5), (6), and (8)), we calculate the tangent stress vector at the wall by performing the projection of the stress vector into the wall tangent direction using the following formula:

$$\boldsymbol{\tau}_w = \boldsymbol{\tau}\cdot\mathbf{n} - ((\boldsymbol{\tau}\cdot\mathbf{n})\cdot\mathbf{n})\,\mathbf{n}, \quad (46)$$

where $\mathbf{n}$ is the unit normal vector at the boundary.

The method proved to be unstable (numerical wiggles appear at the entrance of the channel), especially in the presence of slip, therefore, the slip velocity evolution had to be highly relaxed.

To control the slip velocity growth, a method similar to that of Ref. 4 could also be used (see Appendix C) but with caution since this kind of relaxation is very sensitive to numerical errors when the full tangent stress at the wall is considered. Instead, the classical use of under-relaxation, $u^i_{ws} = Ru^{i-1}_{ws} + (1-R)\,u^i_{ws}$, with $0 < R < 1$, is to be preferred when updating the slip velocity in the iterative procedure. The relaxation factor R can also be a function of the difference between the slip velocity and the velocity at the center of the nearest computational cell, $\left|u^{i-1}_{\mathrm{P}} - u^i_{ws}\right|$, to account for the need of stronger relaxation at the beginning of the iterative process.

The iterative procedure (algorithm) is the same as the one presented before except that at step 3 the slip velocity is obtained making use of Eqs. (5) and (6) or (8) together with Eq. (46).

a. Remark. In regard to the methods proposed above, it is important to emphasise that the simplified method is correct for Newtonian and non-Newtonian fluids in regions of fully developed flow and approximate elsewhere. In addition, it is a very stable method offering no convergence problems. By contrast, the method relying on the full stress equations is valid everywhere but its drawback is that it is unstable, in particular in geometries with singularities. Furthermore, it requires a more refined mesh near the wall than the simplified method, in order to obtain a smooth solution (note that in the Couette flow approximation in the vicinity of the wall, there is a direct relationship between velocity and stress at the wall, while, in this case (full stress tensor at the wall), we need to perform an extrapolation of the stress). Since the simplified method was only analyzed theoretically on the basis of an assumed velocity variation, we next compare its predictions with those by the exact method in order to better assess its validity in regions where the flow is not fully developed.

V. RESULTS AND DISCUSSION

A. Code verification

To validate the implementation of the non-linear slip models, we compare their numerical predictions with the

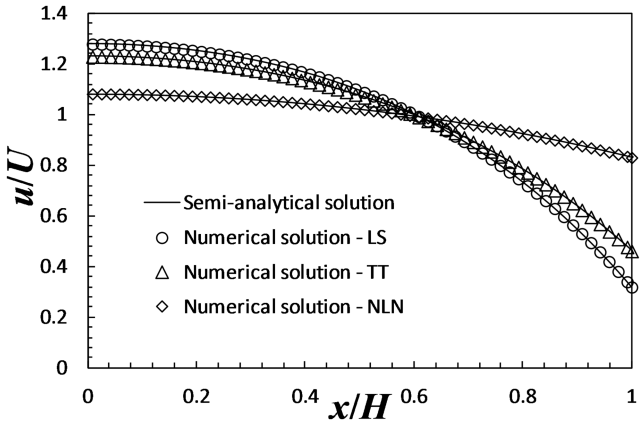

FIG. 4. Comparison between semi-analytical solutions and the simulated results obtained for a fully developed Poiseuille flow, under the influence of three different slip boundary conditions: LS, TT, NLN, for $Wi = 1$, $\varepsilon = 0.25$, $k_{nl}^{'} = 2.53$, and $m = 1.5$ for the NLN slip model, $\alpha^{'} = 0.4$ and $\beta^{'} = 4.0 \times 10^{-4}$ for the LS slip model, and, $c_1^{'} = 0.24$, $c_2 = 0.59 \times 10^{-6}$, $c_3^{'} = 0.024$, $RT = 3.43 \times 10^3$ Jmol^{-1}, and $E = 5.0 \times 10^3$ Jmol^{-1}K^{-1} for the TT slip model.

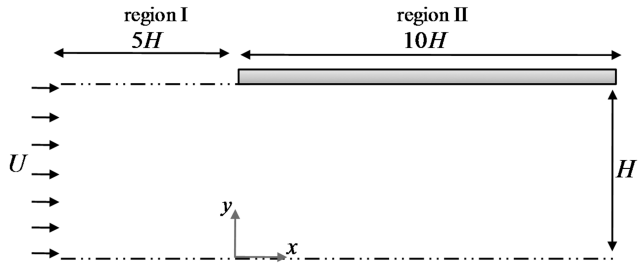

FIG. 5. Schematic representation of the slip-stick geometry.

analytical and semi-analytical solutions for fully developed Poiseuille flow between parallel plates (see Appendix A), with the corresponding simulation results (cf. Fig. 4).

The simulations were performed for the sPTT model with $Wi = 1$ and $\varepsilon = 0.25$, and the slip coefficients used were $k_{nl}^{'} = 2.53$ and $m = 1.5$ for the non-linear Navier slip model, $\alpha^{'} = 0.4$ and $\beta^{'} = 4.0 \times 10^{-4}$ for the LS slip model, and, $c_1^{'} = 0.24$, $c_2 = 0.59 \times 10^{-6}$, $c_3^{'} = 0.024$, $RT = 3.43 \times 10^3$ Jmol^{-1}, and $E = 5.0 \times 10^3$ Jmol^{-1}K^{-1} for the TT slip model. A good agreement between the analytical and numerical results for the three non-linear slip models is seen in the profiles presented in Fig. 4, showing that the implementation of these models is in agreement with the theoretical results (the numerical results were obtained with both SIMPLE-slip and extrapolated full stress tensor, but there were no differences). Nevertheless, note that these numerical results were obtained for a fully developed flow region.

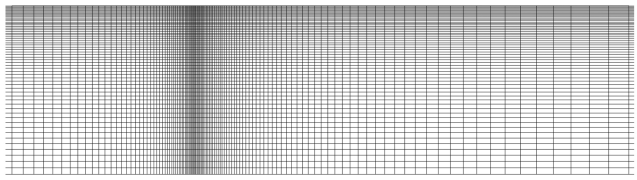

FIG. 6. Detailed view of mesh M3 near the singularity point.

B. Comparison between the numerical methods

In order to compare the two numerical methods (Couette flow assumption and stress tensor extrapolation), we performed simulations for the 2D slip-stick flow shown in Fig. 5, considering the sPTT model.

The computational domain consists of two regions: the inlet region I bounded by two symmetry planes and the outlet region II bounded by a solid wall and a symmetry plane at the top and bottom boundaries, respectively. Variable U stands for the imposed mean velocity and three meshes were used with the geometrical properties described in Table I.

The finest mesh (M4) employed doubles the number of cells of the mesh used in Ref. 5 (M3), for which the results were shown to be mesh independent for the no-slip case at the exit channel. In Table I, fx and fy stand for the ratio between the cell sizes of two consecutive cells while nx and ny stand for the number of cells in the x and y directions, respectively. A zoomed view of mesh M3 can be seen in Fig. 6.

We used the linear Navier slip law, a solvent viscosity ratio of $\beta = \frac{\eta_s}{\eta_s+\eta_p} = \frac{\eta_s}{\eta} = \frac{1}{5}$, $\varepsilon = 0.25$, a constant Reynolds number $Re = \rho UH/\eta = 20$, and a Weissenberg number, $Wi = \lambda U/H = 2$, since a smaller Wi number would possibly hide differences between the two methods. Four different values of the slip coefficient were used, $k_{nl}^{'} = 0$ (the no slip case), $k_{nl}^{'} = 0.0025$, 2.5, and 2500. These results are shown in terms of contour lines for the variables u, v, τ_{xx}, τ_{xy}, and τ_{yy}, for small (Figs. 7(a) and 7(b)) and high (Figs. 8(a) and 8(b)) slip coefficients.

For all the slip coefficients shown in Figs. 7 and 8, we can see that the contour lines obtained by the different methods are almost superimposed, especially for the streamwise (the strongest) velocity component, u. For the transverse velocity component v, there are small differences near the singularity (these differences also occur for the no-slip in a smaller scale and are restricted to the region formed by the two cells used in the linear extrapolation). Note that we are showing the absolute difference between the two methods; therefore, it is expected for the differences to be greater in the transverse velocity component because it shows very small velocity

TABLE I. Mesh characteristics for the slip-stick geometry.

	M1				M2				M3				M4			
Region	f_x	f_y	n_x	n_y	F_x	f_y	n_x	n_y	f_x	f_y	n_x	n_y	f_x	f_y	n_x	n_y
I	0.7901	0.8697	18	15	0.8889	0.9326	36	30	0.9428	0.9657	72	60	0.9710	0.9827	144	120
II	1.1994	0.8697	25	15	1.0952	0.9326	50	30	1.0465	0.9657	100	60	1.0230	0.9827	200	120
Number of cells=				645				2580				10320				41280
$\Delta x_{min}/H = \Delta y_{min}/H =$				0.02				0.01				0.004				0.004

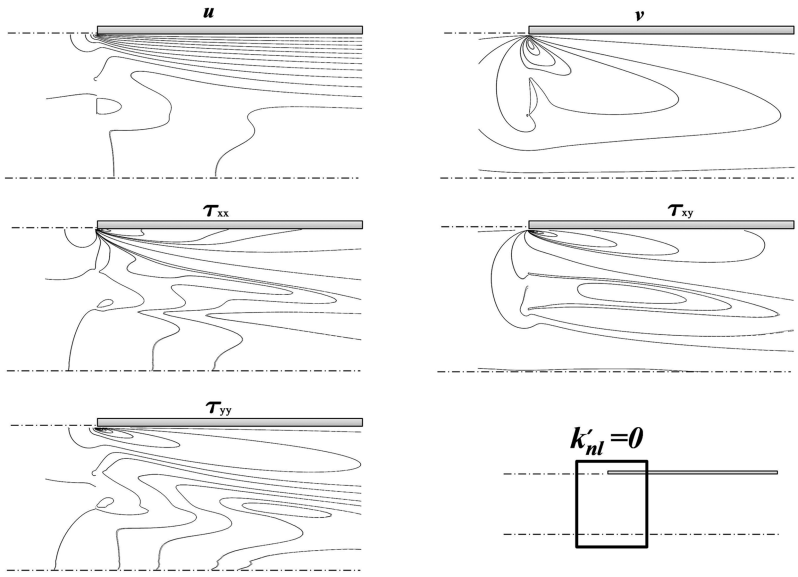

(a)

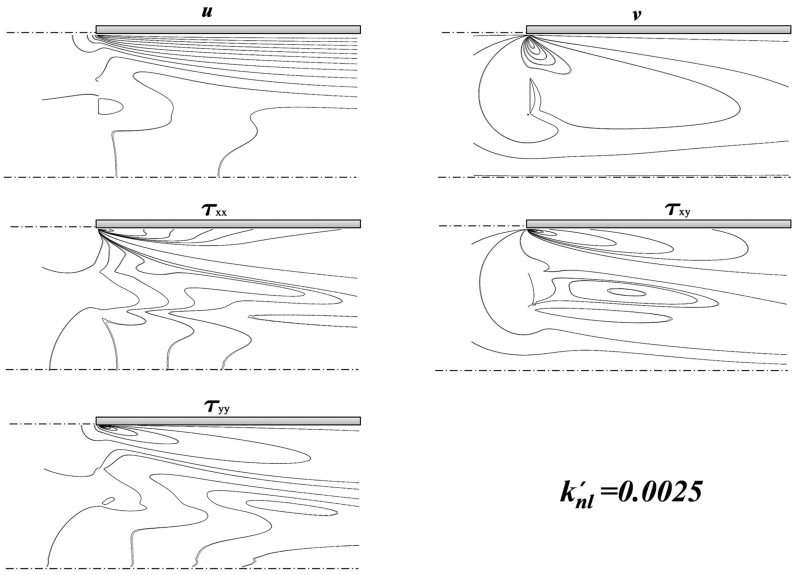

(b)

FIG. 7. Contour lines for the velocity and stress components using the SIMPLE-slip method (solid line) and the extrapolation of the stress vector at the wall (dashed lines) for $\beta = \frac{\eta_s}{\eta_s+\eta_p} = \frac{\eta_s}{\eta} = \frac{1}{5}$, $\varepsilon = 0.25$, $Re = 20$, $Wi = 2$, and no-slip or small slip velocity (a) $k_{nl}^{'} = 0$ and (b) $k_{nl}^{'} = 0.0025$.

values when compared to u. Hence, this absolute difference corresponds to a smaller relative difference between the two methods. Far from the wall, there are also some small differences due to the coarser mesh there.

For the no-slip and small slip velocity (Figs. 7(a) and 7(b)) and for the high slip velocity cases (Fig. 8(b)), there is a good agreement between the stress contours obtained with the two different methods, whereas for $k_{nl}^{'} = 2.5$, some small differences are encountered in the vicinity of the wall for τ_{xx}, τ_{xy}, and τ_{yy}. Mesh refinement tests showed that these differences are restricted to a thin near wall layer in the cells used for the extrapolation of the stress tensor, hence, the differences should be suppressed with further mesh refinement.

Therefore, we may conclude that the approximation used in the SIMPLE-slip method is a good approximation for the tangent stress at the wall, at least for the flow characteristics studied here, with the main differences between the two methods restricted to a small area in the vicinity of the wall.

C. Elasticity effects

To evaluate the influence of the slip velocity in the dynamics of viscoelastic fluid flow in a geometry that possesses a singular point, we performed additional simulations. For the sake of compactness, only the results for the NLN model are presented. These simulations were carried out using the extrapolation of the stress tensor method, but, since no considerable flow differences were obtained between the two numerical methods, the SIMPLE-slip technique could have also been used, especially because it is more stable.

The simulations were performed for the sPTT model with a solvent viscosity ratio of $\beta = \frac{1}{5}$ and $\varepsilon = 0.25$ at a constant Reynolds number $Re = 20$ and a varying Weissenberg number, $Wi = \lambda U/H \in \{0.25, 0.5, 1.0, 2.0\}$. For the linear slip model, implemented via Eq. (14), convergence could be achieved for all the Weissenberg numbers analyzed. As expected, an easier convergence was obtained for higher slip velocities (high slip

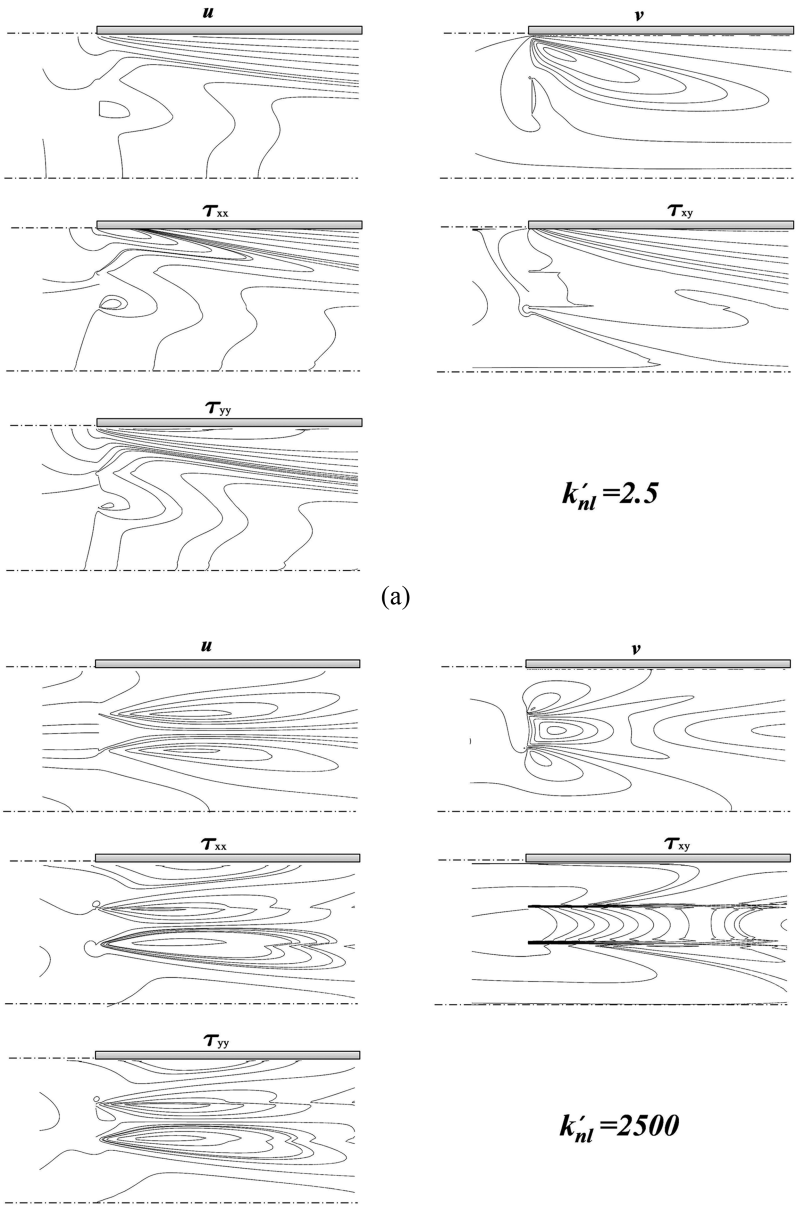

FIG. 8. Contour lines for the velocity and stress components using the SIMPLE-slip method (solid line) and the extrapolation of the stress vector at the wall (dashed lines) for $\beta = \frac{1}{5}$, $\varepsilon = 0.25$, $Re = 20$, $Wi = 2$, and high slip velocity, (a) $k_{nl}^{'} = 2.5$ and (b) $k_{nl}^{'} = 2500$.

coefficients) because the slip velocity reduces the effect of the singularity. For the nonlinear model, the results were qualitatively similar to those obtained with the linear slip model except that convergence was more difficult, not because of the singularity but due to the method employed, as explained in Ferris *et al.*[4]

In order to quantify the effect of slip velocity on the flow patterns, the streamlines for two different values of the slip coefficient are shown in Fig. 9. For the case $k_{nl}^{'} = 0.0025$ (small slip velocity), curved streamlines appear in the slip-friction region because of the fluid viscosity effects and the restriction promoted by the wall (Fig. 9(a)) that induce flow deceleration. The streamlines for the higher slip coefficient, $k_{nl}^{'} = 2500$, are almost horizontal because for this case the wall restrictive effect is negligible, thus the curvature of the streamlines tends to disappear (Fig. 9(b)) due to the negligible deceleration.

The stress field was also analyzed, together with the characterization of the flow type parameter, ξ, defined as[24]

$$\xi = \frac{|\mathbf{D}| - |\mathbf{\Omega}|}{|\mathbf{D}| + |\mathbf{\Omega}|}, \tag{47}$$

where $|\mathbf{D}|$ and $|\mathbf{\Omega}|$ represent the magnitudes of the rate of deformation and vorticity tensors, respectively, given by

$$\mathbf{D} = \frac{1}{2}\left[\nabla \mathbf{u} + (\nabla \mathbf{u})^{\mathrm{T}}\right], \quad \mathbf{\Omega} = \frac{1}{2}\left[\nabla \mathbf{u} - (\nabla \mathbf{u})^{\mathrm{T}}\right], \tag{48}$$

which can be calculated as

$$\begin{aligned} |\mathbf{D}| &= \sqrt{\frac{1}{2}\left(\mathbf{D} : \mathbf{D}^{\mathrm{T}}\right)} = \sqrt{\frac{1}{2}\sum_i \sum_j D_{ij}^2}, \\ |\mathbf{\Omega}| &= \sqrt{\frac{1}{2}\left(\mathbf{\Omega} : \mathbf{\Omega}^{\mathrm{T}}\right)} = \sqrt{\frac{1}{2}\sum_i \sum_j \Omega_{ij}^2}. \end{aligned} \tag{49}$$

The flow type parameter varies from $\xi = -1$, which corresponds to solid-like rotation, up to $\xi = 1$, for pure extensional flow. Shear flow is characterized by $\xi = 0$. In Fig. 10, we show the contour plots of the τ_{xx} component (polymeric

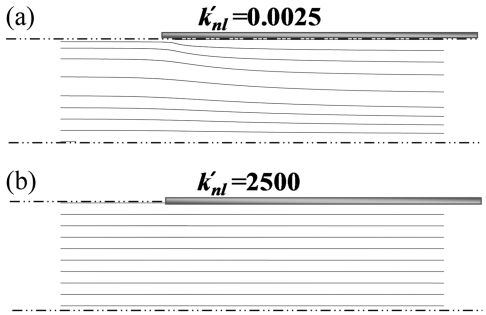

FIG. 9. Computed streamlines for the sPTT model with a solvent viscosity ratio of $\beta = \frac{1}{5}$ and $\varepsilon = 0.25$ at a constant Reynolds number $Re = 20$, $Wi = 2$, and (a) $k'_{nl} = 0.0025$ and (b) $k'_{nl} = 2500$.

contribution) and flow type parameter, ξ, for three different slip coefficients, whereas Figs. 11 and 12 show the corresponding contour plots for τ_{xy} and τ_{yy}. For lower slip velocity coefficients, the region of shear-dominant flow is concentrated near the channel wall, while the extension flow is dominant close to the symmetry boundaries. Note also that the region of extension-dominated flow extends downstream as one approaches the outlet channel centerline because the momentum diffusion effect takes longer to act when the shear rate is low. Increasing the slip velocity coefficient enlarges the shear-dominated flow region also in the vicinity of the stagnation point, because the suppression of the wall braking effect tends to reduce the flow extensional region deformation, and thus increases the relevance of shear. Hence for higher slip velocity coefficients, the extension-dominant flow is limited to a thinner region near the walls, which very slowly and progressively grows downstream, again a consequence of the suppression of the wall braking effect. This is actually the region that at small slip coefficients exists near the center of the channel, which moves towards the wall, and becomes thinner, as the slip coefficient increases. The τ_{xx} component changes drastically with the increase of slip. Notice that for the Newtonian fluid case, with no-slip, this stress component is negative (compressive) in the region of fluid near the wall, as explained in Ref. 5, whereas for viscoelastic fluids, in the presence of low slip velocity (Fig. 10(a)), this stress component becomes positive (traction).

However, on increasing the slip velocity, the normal stress τ_{xx} near the wall becomes negative, as verified for Newtonian fluids (Figure 10(c) and Ref. 5). This happens because of the low slip coefficients and the restrictive effect of the wall noticed far upstream, promoting a significant deceleration of the fluid close to the upper boundary at the inlet region. Then, at the outlet region, the fluid is accelerated (to achieve a fully developed velocity profile) promoting the appearance of positive normal stresses. For high slip coefficients, the restrictive effect of the wall is much smaller, leading to a smoother evolution of the velocity that is progressively and slowly reduced near the wall, with the consequent negative normal stresses. For the τ_{xy} component, on increasing the slip coefficient, the negative shear stress values decrease in magnitude in the wall region, as shown in Fig. 11(c). This happens because the velocity profile tends to a plug, which corresponds to a negligible tangent stress as the slip velocity increases (cf. Figs. 11(b) and 11(c)).

For the contour plots of τ_{yy}, shown in Fig. 12, the qualitative behavior is essentially the same on increasing the slip velocity but a reduction in magnitude is visible again associated with the progression towards a plug velocity profile. Interestingly, for the higher slip velocity coefficient, the contour plot of τ_{yy} is similar to the contour plot of τ_{xx}, but with opposite sign, as also happens for Newtonian fluids.[5]

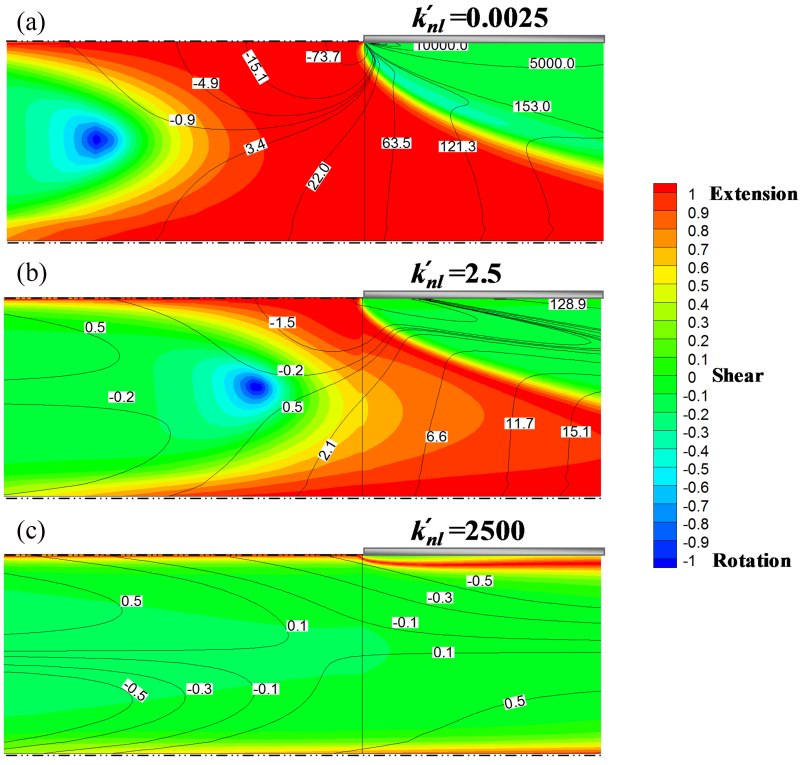

FIG. 10. Representation of contour lines ($\tau_{xx}[Pa]$) superimposed with the flow type ξ contours (in color) for the linear slip model: (a) $k'_{nl} = 0.0025$, (b) $k'_{nl} = 2.5$, and (c) $k'_{nl} = 2500$. sPTT model with a solvent viscosity ratio of $\beta = \frac{1}{5}$ and $\varepsilon = 0.25$ at a constant Reynolds number $Re = 20$ and $Wi = 2$.

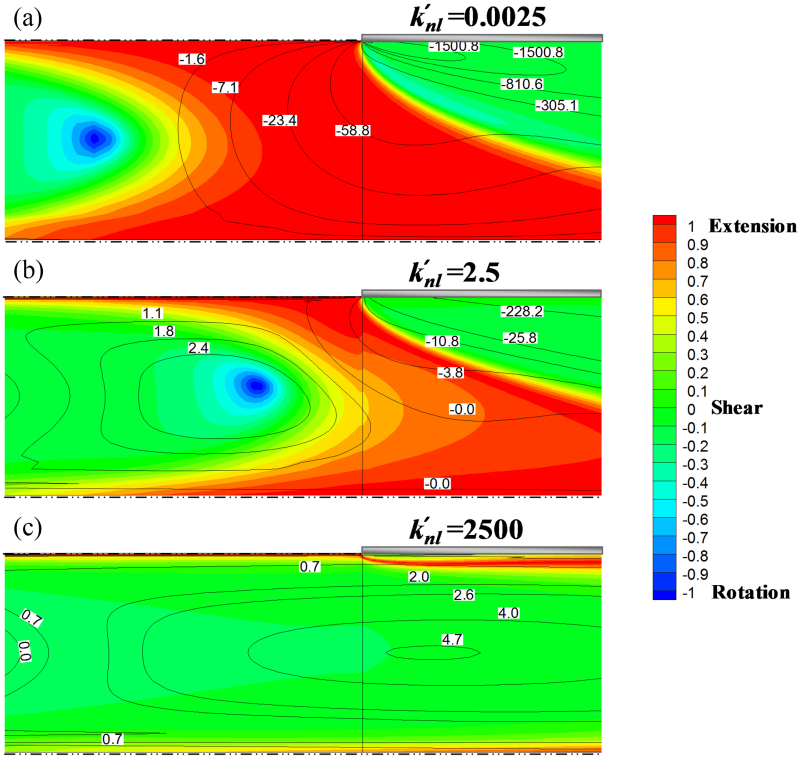

FIG. 11. Representation of contour lines $\left(\tau_{xy}[Pa]\right)$ superimposed with the flow type ξ contours (in color) for the linear slip model: (a) k'_{nl} = 0.0025, (b) k'_{nl} = 2.5, and (c) k'_{nl} = 2500. sPTT model with a solvent viscosity ratio of $\beta = \frac{1}{5}$ and $\varepsilon = 0.25$ at a constant Reynolds number $Re = 20$ and $Wi = 2$.

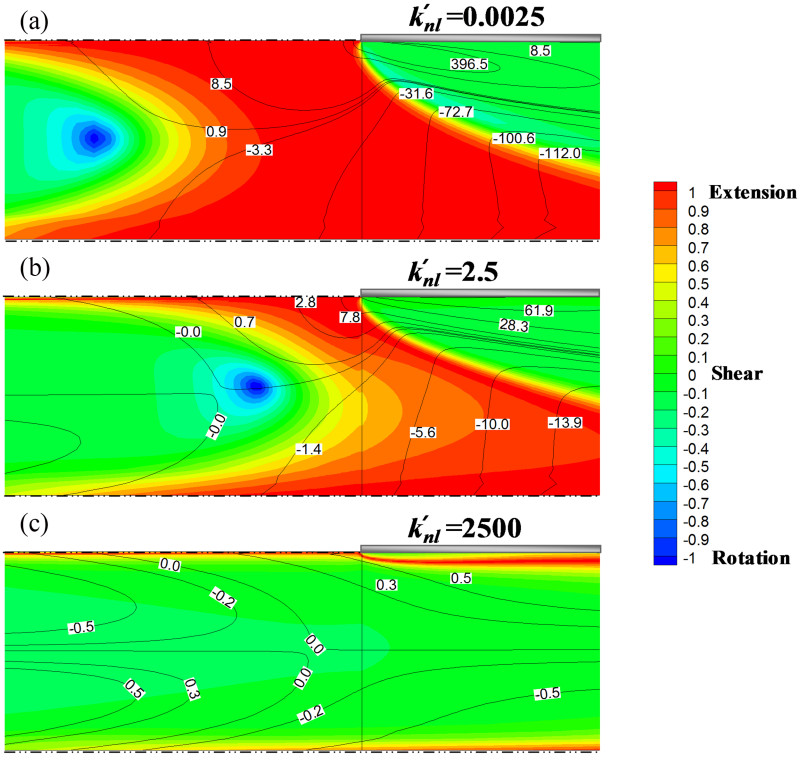

FIG. 12. Representation of contour lines $\left(\tau_{yy}[Pa]\right)$ superimposed with the flow type ξ contours (in color) for the linear slip model: (a) k'_{nl} = 0.0025, (b) k'_{nl} = 2.5, and (c) k'_{nl} = 2500. sPTT model with a solvent viscosity ratio of $\beta = \frac{1}{5}$ and $\varepsilon = 0.25$ at a constant Reynolds number $Re = 20$ and $Wi = 2$.

VI. CONCLUSIONS

In this work, the numerical implementation of the slip boundary condition in a viscoelastic flow solver, based on the finite volume method, was described for three different slip velocity models. Two different implementations were used and compared, the SIMPLE-slip formulation and a formulation where the full stress vector is considered at the wall. The results obtained with both approaches are in general similar, with the exception of small differences near the walls, where the slip boundary conditions are employed. However, the SIMPLE-slip method proved to be more stable. The code was then employed to study the effect of the slip velocity on the slip-stick flow. This study allowed us to verify that the shear dominant regions, which are located near the wall, for low slip magnitudes, expand to cover the majority of the flow channel, when slip increases. Moreover, all the stress component magnitudes reduce with the slip

growth, mainly due to the suppression of the wall restrictive effect.

Semi analytical solutions were obtained for the 2D fully developed Poiseuille flow of viscoelastic fluid following the simplified Phan-Thien-Tanner model, under the influence of Thomson and Troian, Lau and Schowalter, and nonlinear Navier slip models. For a specific range of model parameters, an analytical solution was devised for the same problem with the Lau and Schowalter slip model.

ACKNOWLEDGMENTS

The authors acknowledge funding from FEDER and Fundacão para a Ciência e Tecnologia (FCT), Portugal, through Project Nos. PTDC/EMS-ENE/3362/2014, PTDC/EQU-FTT/113811/2009, and PTDC/EME-MFE/113988/2009 and FEDER, via FCT, under the Project No. UID/CTM/50025/2013. L.L.F. would like to thank FCT for the funding through the Scholarship No. SFRH/BPD/100353/2014.

APPENDIX A: ANALYTICAL SOLUTIONS OF FULLY DEVELOPED CHANNEL FLOW FOR THE sPTT AND FENE-P VISCOELASTIC MODELS WITH NONLINEAR WALL SLIP BOUNDARY CONDITIONS

Considering a 2D Cartesian coordinate system (x, y) and a fully developed Poiseuille flow (see Fig. 1), the governing equations can be simplified because

$$\partial/\partial x = 0 \text{ (except for pressure)}, \; v = 0, \; \partial p/\partial y = 0. \quad \text{(A1)}$$

This leads to the following simplification in the momentum equation:

$$\tau_{xy} = p_x y, \quad \text{(A2)}$$

where p_x stands for the pressure gradient in the x direction and τ_{xy} is the shear stress.

Under the same assumptions, the system of rheological constitutive equations for the simplified PTT model can be simplified to

$$f\left(\tau_{xx}+\tau_{yy}\right)\tau_{xx} = 2\lambda\tau_{xy}\left(\frac{du}{dy},\right) \quad \text{(A3a)}$$

$$f\left(\tau_{xx}+\tau_{yy}\right)\tau_{yy} = 0, \quad \text{(A3b)}$$

$$f\left(\tau_{xx}+\tau_{yy}\right)\tau_{xy} = \eta\left(\frac{du}{dy}\right)+\lambda\tau_{yy}\left(\frac{du}{dy}\right). \quad \text{(A3c)}$$

From Eq. (A3b), we obtain $\tau_{yy} = 0$ since $f\left(\tau_{xx}+\tau_{yy}\right) \neq 0$.

Dividing Eq. (A3a) by Eq. (A3c), the former becomes $\tau_{xx} = (2\lambda/\eta)\left(\tau_{xy}\right)^2$. If Eqs. (A3a)–(A3c) are combined with the momentum equation, and after normalization, the following system is obtained:

$$\tau_{xy}^{'} = p_x^{'}y^{'}, \quad \text{(A4a)}$$

$$\tau_{xx}^{'} = 2Wi\left(p_x^{'}y^{'}\right)^2, \quad \text{(A4b)}$$

$$\tau_{yy}^{'} = 0, \quad \text{(A4c)}$$

$$\left(\frac{du^{'}}{dy^{'}}\right) = p_x^{'}y^{'}+2\varepsilon Wi^2\left(p_x^{'}y^{'}\right)^3 \quad \text{(A4d)}$$

with length, velocity, and stresses scaled with H, U, and $\eta U/H$, respectively, where U is the mean streamwise velocity, H is the channel half width (see Fig. 1), and $Wi = \lambda U/H$ is the Weissenberg number.

The boundary conditions at the lower $\left(y^{'} = -1\right)$ and upper walls $\left(y^{'} = +1\right)$ are written in a dimensionless form as

$$u_{ws}^{'} = u^{'}(\pm 1) = -k_{nl}^{'}p_x^{'}\left|p_x^{'}\right|^{m-1}, \quad \text{(A5)}$$

$$u_{ws}^{'} = u^{'}(\pm 1) = \frac{-\alpha^{'}p_x^{'}}{\sqrt{1-\beta^{'}\left|p_x^{'}\right|}}, \quad \text{(A6)}$$

$$u_{ws}^{'} = u^{'}(\pm 1) = -c_1^{'}p_x^{'}\left|p_x^{'}\right|^{m-1}\left[1-c_2\tanh\left(\frac{E-c_3^{'}\left|p_x^{'}\right|}{RT}\right)\right], \quad \text{(A7)}$$

for the nonlinear Navier, the TT, and LS slip models, respectively, and $k_{nl}^{'} = kU^{m-1}(\eta/H)^m$, $\alpha^{'} = \alpha(\eta/H)$, $\beta^{'} = \beta(\eta U/H)$, $c_1^{'} = c_1U^{m-1}$, and $c_3^{'} = c_3(\eta U/H)$.

Integrating Eq. (A4d) gives

$$u^{'}\left(y^{'}\right) = 0.5p_x^{'}y^{'2}+0.5\varepsilon Wi^2p_x^{'3}y^{'4}+d, \;\; d\in\mathbb{R}, \quad \text{(A8)}$$

where we have two unknowns, the dimensionless pressure gradient, $p_x^{'}$ and the integration constant d. To find d, we can make use of the slip boundary condition $u_{ws}^{'}$ given by Eqs. (A5)–(A7). Therefore, the solution for the direct problem is given by

$$u^{'}\left(y^{'}\right) = 0.5p_x^{'}\left(y^{'2}-1\right)+0.5\varepsilon Wi^2p_x^{'3}\left(y^{'4}-1\right)+u_{ws}^{'}. \quad \text{(A9)}$$

By applying a constant flow rate per unit depth, $Q = 2UH$, and integrating Eq. (A9) over half-width of the channel

$$\int_0^1 u^{'}\left(y^{'}\right)dy^{'} = 1, \quad \text{(A10)}$$

the following equation is obtained to determine the other unknown, the dimensionless pressure gradient $p_x^{'}$,

$$(-2/5)\,\varepsilon Wi^2p_x^{'3}-(1/3)\,p_x^{'}-1+u_{ws}^{'} = 0. \quad \text{(A11)}$$

The strong nonlinearity of Eq. (A11) in $p_x^{'}$, mainly due to the $u_{ws}^{'}$ term, makes it difficult to find closed form solutions for this equation.

For the nonlinear Navier slip model, these solutions were already reported in the literature and can be found in Ref. 25. For the other two slip models, one can only prove the existence and uniqueness of a solution and provide the range where the solution lies (for the LS slip model an approximate particular solution can still be obtained). In this way, it is easy to find the solution using a numerical method to solve the corresponding transcendent equations. For this purpose, it is useful to identify the solution range that is given below for the TT and LS slip models.

Without loss of generality we assume that the velocities are positive.

1. TT slip model

Let $f\left(p_x^{'}\right) = (-2/5)\,\varepsilon Wi^2 p_x^{'3} - (1/3)\,p_x^{'} - 1 - \frac{\alpha^{'} p_x^{'}}{\sqrt{1+\beta^{'} p_x^{'}}}$, then

$$\frac{df\left(p_x^{'}\right)}{dp_x^{'}} = \frac{-6}{5}\varepsilon Wi^2 p_x^{'2} - \frac{1}{3} - \frac{\alpha^{'}\sqrt{1+\beta^{'}p_x^{'}}}{1+\beta^{'}p_x^{'}} + \frac{\alpha\beta p_x^{'}}{2\left(1+\beta^{'}p_x^{'}\right)\sqrt{1+\beta^{'}p_x^{'}}} < 0. \tag{A12}$$

Since $f(-3) > 0$ and $f(0) = -1 < 0$ (providing that $\beta^{'} < 1/3$) and $\frac{df\left(p_x^{'}\right)}{dp_x^{'}} < 0$, the intermediate value theorem together with Rolle theorem guarantees the existence of a unique solution in the range $[-3, 0]$.

2. LS slip model

Let $g\left(p_x^{'}\right) = (-2/5)\,\varepsilon Wi^2 p_x^{'3} - (1/3)\,p_x^{'} - 1 + c_1^{'}\left(-p_x^{'}\right)^m \left[1 - c_2 \tanh\left(\frac{E+c_3^{'}\left(p_x^{'}\right)}{RT}\right)\right]$, then

$$\frac{dg\left(p_x^{'}\right)}{dp_x^{'}} = \frac{-6}{5}\varepsilon Wi^2 p_x^{'2} - \frac{1}{3} - mc_1^{'}\left(-p_x^{'}\right)^{m-1} \times\left[1 - c_2\tanh\left(\frac{E+c_3^{'}\left(p_x^{'}\right)}{RT}\right)\right] - \frac{c_1^{'}c_2c_3^{'}\left(-p_x^{'}\right)^m}{RT\cosh^2\left(\frac{E+c_3^{'}\left(p_x^{'}\right)}{RT}\right)} < 0. \tag{A13}$$

Since $g(-3) > 0$ and $g(0) = -1 < 0$ and $\frac{df\left(p_x^{'}\right)}{dp_x^{'}} < 0$, again there is a unique solution in the range $[-3, 0]$.

For small values of the tanh argument, $\frac{E+c_3^{'}\left(p_x^{'}\right)}{RT} \ll 1$, we can approximate $\tanh\left(\frac{E+c_3^{'}\left(p_x^{'}\right)}{RT}\right)$ as $\frac{E+c_3^{'}\left(p_x^{'}\right)}{RT}$ (linear) or as $\frac{E+c_3^{'}\left(p_x^{'}\right)}{RT} - \frac{1}{3}\left(\frac{E+c_3^{'}\left(p_x^{'}\right)}{RT}\right)^3$ (truncated series expansion). With these approximations, and assuming $m = 1$ in Eq. (A11), the following equation is obtained:

$$-\frac{2}{5}\varepsilon Wi^2 p_x^{'3} + \frac{c_1^{'}c_2c_3^{'}}{RT}p_x^{'2} + \left(-\frac{1}{3} - c_1^{'} + \frac{c_1^{'}c_2E}{RT}\right)p_x^{'} - 1 = 0. \tag{A14}$$

This equation can be written in a more compact form as

$$p_x^{'3} + a_1 p_x^{'2} + a_2 p_x^{'} + a_3 = 0, \tag{A15}$$

and the relevant real solution is given by the Cardano-Tartaglia formula

$$p_x^{'} = \sqrt[3]{-\frac{P}{2} + \sqrt{\frac{P^2}{4} + \frac{S^3}{27}}} + \sqrt[3]{-\frac{P}{2} - \sqrt{\frac{P^2}{4} + \frac{S^3}{27}}} - \frac{a_1}{3} \tag{A16}$$

with

$$\begin{aligned} a_1 &= -\frac{5c_1^{'}c_2c_3^{'}}{2RT}, \\ a_2 &= \frac{-\frac{1}{3} - c_1^{'} + \frac{c_1^{'}c_2E}{RT}}{-\frac{2}{5}\varepsilon Wi^2}, \\ a_3 &= \left(\frac{2}{5}\varepsilon Wi^2\right)^{-1}, \\ P &= a_3 - \frac{a_1a_2}{3} + \frac{2a_1^3}{27}, \\ S &= a_2 - \frac{a_1^2}{3}. \end{aligned} \tag{A17}$$

The previous equations are also applicable for the FENE-P constitutive equation provided the appropriate change of variables is used, as discussed in Ref. 26.

APPENDIX B: NUMERICAL IMPLEMENTATION OF THE TT AND LS SLIP MODELS USING A SEMI-IMPLICIT METHOD BASED ON THE SOLUTION OF A TRANSCENDENT EQUATION

The benefit of using this method was already explained in Ref. 4 for the nonlinear Navier slip model. Here we only show how to apply it for the TT and LS slip velocity models.

The slip boundary conditions could be implemented considering an implicit slip velocity on both sides of the equation for each of the wall boundary cells at each iteration i

$$u_{ws}^{i} = \alpha\mu\left(\delta n^2 - \delta n\beta\mu\left|u_{\mathrm{P}}^{i-1} - u_{ws}^{i}\right|\right)^{-1/2}\left(u_{\mathrm{P}}^{i-1} - u_{ws}^{i}\right), \tag{B1}$$

$$u_{ws}^{i} = \frac{c_1\mu^m}{\delta n^m}\left(u_{\mathrm{P}}^{i-1} - u_{ws}^{i}\right)\left|u_{\mathrm{P}}^{i-1} - u_{ws}^{i}\right|^{m-1} \times\left[1 - c_2\tanh\left(\frac{E}{RT} - \frac{c_3\mu}{\delta n\,RT}\left|u_{\mathrm{P}}^{i-1} - u_{ws}^{i}\right|\right)\right], \tag{B2}$$

and then use a numerical method to find the solution of these transcendent equations (Eq. (B1) for the TT and Eq. (B2) for the LS slip models).

The iterative procedure is very similar to that in Section III, except that step 3 is now: "3. Compute the slip velocity by solving the transcendent equation for the boundary (Eq. (B1) for the TT model and Eq. (B2) for the LS model)."

The bisection method was the selected algorithm to find the roots of these equations. In the overall numerical procedure, for each wall boundary cell and at each iteration i, the solution is chosen after n internal iterations (bisection method iterations) such that $(b-a)/2^n$ is below a given error ($[a; b]$ are the initial bounds for the solution u_{ws}^{i}).

For these two slip boundary conditions, it can be proved analytically that a unique solution, u_{ws}^{i}, exists and that this solution verifies the condition $u_{ws}^{i} < u_{\mathrm{P}}^{i-1}$.

1. Proof of existence of a unique solution for the LS model

First, the intermediate value theorem will be used to demonstrate the existence of the solution, and then, with the Rolle theorem, we will prove its uniqueness.

We want to prove that

$$\exists\left(u_{ws}^{i}\right)^{1}:\ u_{ws}^{i}=\frac{c_1\mu^m}{\delta n^m}\left(u_{\mathrm{P}}^{i-1}-u_{ws}^{i}\right)\left|u_{\mathrm{P}}^{i-1}-u_{ws}^{i}\right|^{m-1}\left[1-c_2\tanh\left(\frac{E}{RT}-\frac{c_3\mu}{\delta n\,RT}\left|u_{\mathrm{P}}^{i-1}-u_{ws}^{i}\right|\right)\right]$$
$$\wedge 0\le\left|u_{ws}^{i}\right|\le\left|u_{\mathrm{P}}^{i-1}\right|,\ \ \forall c_1,\,c_2,\,c_3,\,RT,\,m,\,E,\,\delta n,\,u_P^{i-1}\in\mathbb{R}_0^+. \tag{B3}$$

Without the loss of generality assume that u_{ws}^{i} and u_{P}^{i-1} are both positive.

Let us create a function $f(u_{ws}^{i})$ given by

$$f\left(u_{ws}^{i}\right)=u_{ws}^{i}-\frac{c_1\mu^m}{\delta n^m}\left(u_{\mathrm{P}}^{i-1}-u_{ws}^{i}\right)^m\left[1-c_2\tanh\left(\frac{E}{RT}-\frac{c_3\mu}{\delta n\,RT}\left(u_{\mathrm{P}}^{i-1}-u_{ws}^{i}\right)\right)\right]. \tag{B4}$$

Since $f(u_{\mathrm{P}}^{i-1})f(0)<0$ and $f(\cdot)$ is a real-valued continuous function on the interval $\left[0;\,u_{\mathrm{P}}^{i-1}\right]$, the intermediate value theorem implies that $\exists u_{ws}^{i}:\ f(u_{ws}^{i})=0$. Then, because $f'\left(u_{ws}^{i}\right)<0$ for $u_{ws}^{i}\in\left[0;\,u_{\mathrm{P}}^{i-1}\right]$, using the Rolle theorem we conclude that the solution is unique.

For $m=1$, we can narrow down the range where the solution lies.

Assuming $c_2\tanh\left(\frac{E}{RT}-\frac{c_3\mu}{\delta n\,RT}\left|u_{\mathrm{P}}^{i-1}-u_{ws}^{i}\right|\right)<1$, then

$$u_{ws}^{i}=\frac{c_1\mu}{\delta n}\left(u_{\mathrm{P}}^{i-1}-u_{ws}^{i}\right)\left[1-c_2\tanh\left(\frac{E}{RT}-\frac{c_3\mu}{\delta n\,RT}\left|u_{\mathrm{P}}^{i-1}-u_{ws}^{i}\right|\right)\right]\le\frac{c_1\mu}{\delta n}\left|u_{\mathrm{P}}^{i-1}-u_{ws}^{i}\right| \tag{B5}$$

meaning that

$$u_{ws}^{i}<\frac{\frac{c_1\mu}{\delta n}}{1+\frac{c_1\mu}{\delta n}}u_P^{i-1}. \tag{B6}$$

In general, for u_{ws}^{i} positive or negative, we have

$$\left|u_{ws}^{i}\right|<\frac{\frac{c_1\mu}{\delta n}}{1+\frac{c_1\mu}{\delta n}}\left|u_P^{i-1}\right|. \tag{B7}$$

The initial range for the bisection method is given by

$$[a,\,b]\equiv\begin{cases}\left[0,\ \frac{\frac{c_1\mu}{\delta n}}{1+\frac{c_1\mu}{\delta n}}\left|u_P^{i-1}\right|\right] & if\ \ m=1\\ \left[0,\ \left|u_P^{i-1}\right|\right] & if\ \ m\neq 1\end{cases}. \tag{B8}$$

For the TT model, we can use a similar procedure to prove the existence of a unique solution $\left|u_{ws}^{i}\right|\in\left[0;\,\left|u_P^{i-1}\right|\right]$. Furthermore, we have that

$$u_{ws}^{i}=\alpha\frac{\mu}{\delta n}\left(1-\frac{\beta\mu}{\delta n}\left|u_{\mathrm{P}}^{i-1}-u_{ws}^{i}\right|\right)^{-1/2}\left(u_{\mathrm{P}}^{i-1}-u_{ws}^{i}\right). \tag{B9}$$

Since $\left(1-\frac{\beta\mu}{\delta n}\left|u_{\mathrm{P}}^{i-1}-u_{ws}^{i}\right|\right)^{-1/2}<1$, this sets a new initial range for the bisection method given by

$$[a,\,b]\equiv\left[\frac{\alpha\frac{\mu}{\delta n}}{1+\alpha\frac{\mu}{\delta n}}\left|u_P^{i-1}\right|,\ \left|u_P^{i-1}\right|\right]. \tag{B10}$$

By using these ranges as initial guesses for the bisection method (used to obtain the solutions of these transient equations), we gain computational time.

APPENDIX C: GENERALIZED IMPLEMENTATION OF SLIP MODELS

Provided we can express the slip velocity as a function of the wall shear stress and assuming a one-dimensional flow, the slip velocity u_{ws} can be written as a function of the difference $\left|u_{\mathrm{p}}-u_{ws}\right|$, i.e., $u_{ws}=\pm f\left(\left|u_{\mathrm{p}}-u_{ws}\right|\right)$, where the $\pm$ depends on the direction of the slip velocity and u_{p} is the velocity at the computational cell adjacent to the wall. This function can be multiplied by $\pm\left(u_{\mathrm{p}}^{i-1}-u_{ws}^{i}\right)/\left|u_{\mathrm{p}}^{i-1}-u_{ws}^{i-1}\right|$ and solved in a semi-implicit manner. In the iterative procedure, only the slip velocity in the numerator comes from the actual iteration, so the general slip boundary condition can be written as

$$u_{ws}^{i}=\left[\frac{f\left(\left|u_{\mathrm{p}}^{i-1}-u_{ws}^{i-1}\right|\right)}{\left|u_{\mathrm{p}}^{i-1}-u_{ws}^{i-1}\right|+f\left(\left|u_{\mathrm{p}}^{i-1}-u_{ws}^{i-1}\right|\right)}\right]u_{\mathrm{P}}^{i-1}. \tag{C1}$$

For the three slip boundary conditions studied here, the function $f\left(\left|u_{\mathrm{p}}^{i-1}-u_{ws}^{i-1}\right|\right)$ is given by

$$f\left(\left|u_{\mathrm{p}}^{i-1}-u_{ws}^{i-1}\right|\right)=k\left(\frac{\mu(\dot\gamma)_w}{\delta n}\right)^m\left|u_{\mathrm{p}}^{i-1}-u_{ws}^{i-1}\right|^m \tag{C2}$$

for the NNS model, by

$$f\left(\left|u_{\mathrm{p}}^{i-1}-u_{ws}^{i-1}\right|\right)=\alpha\left(1-\frac{\beta\mu}{\delta n}\left|u_{\mathrm{p}}^{i-1}-u_{ws}^{i-1}\right|\right)^{-1/2}\frac{\mu}{\delta n}\left|u_{\mathrm{p}}^{i-1}-u_{ws}^{i-1}\right| \tag{C3}$$

for the TT slip model, and by

$$f\left(\left|u_{\mathrm{p}}^{i-1}-u_{ws}^{i-1}\right|\right)=\frac{c_1\mu^m}{\delta n^m}\left|u_{\mathrm{p}}^{i-1}-u_{ws}^{i-1}\right|^m\times\left[1-c_2\tanh\left(\frac{E}{RT}-\frac{c_3\mu}{\delta n\,RT}\left|u_{\mathrm{p}}^{i-1}-u_{ws}^{i-1}\right|\right)\right] \tag{C4}$$

for the LS slip velocity model.

[1] H. Potente, H. Ridder, and R. Cunha, "Global concept for describing and investigation of wall slip effects in the extrusion process," Macromol. Mater. Eng. **287**(11), 836–842 (2002).

[2] E. Mitsoulis, I. Kazatchkov, and S. G. Hatzikiriakos, "The effect of slip in the flow of a branched PP melt: Experiments and simulations," Rheol. Acta **44**, 418–426 (2005).

[3] M. M. Denn, "Extrusion instabilities and wall slip," Annu. Rev. Fluid Mech. **33**, 265–287 (2001).

[4] L. L. Ferrás, J. M. Nóbrega, and F. T. Pinho, "Implementation of slip boundary conditions in the finite volume method: New techniques," Int. J. Numer. Methods Fluids **72**(7), 724–747 (2013).

[5] P. J. Oliveira, F. T. Pinho, and G. A. Pinto, "Numerical simulation of nonlinear elastic flows with a general collocated finite-volume method," J. Non-Newtonian Fluid Mech. **79**, 1–43 (1998).

[6] N. Phan-Thien and R. I. Tanner, "A new constitutive equation derived from network theory," J. Non-Newtonian Fluid Mech. **2**(4), 353–365 (1977).

[7] N. Phan-Thien, "A nonlinear network viscoelastic model," J. Rheol. **22**, 259 (1978).

[8] W. Schowalter, "The behaviour of complex fluids at solid boundaries," J. Non-Newtonian Fluid Mech. **29**, 25–36 (1988).

[9]S. G. Hatzikiriakos, "A slip model for linear polymers based on adhesive failure," Int. Polym. Process. **8**, 135–142 (1993).
[10]ANSYS, ANSYS Polyflow Manual, Implementation of Boundary Conditions, 2011.
[11]P. Thomson and S. Troian, "A general boundary condition for liquid flow at solid surfaces," Nature **389**, 360–362 (1997).
[12]H. Lau and W. Schowalter, "A model for adhesive failure of viscoelastic fluids during flow," J. Rheol. **30**, 193–206 (1986).
[13]R. B. Bird, R. C. Armstrong, O. Hassager, *Dynamics of Polymeric Liquids: Fluid Mechanics*, 2nd ed. (John Wiley & Sons, New York, 1987), Vol. 1.
[14]M. Mathews and J. Hill, "Newtonian flow with nonlinear Navier boundary condition," Acta Mech. **191**, 195–217 (2007).
[15]J. Uspensky, *Theory of Equations* (McGraw-Hill, New York, 1948), Vol. 72.
[16]P. J. Oliveira and F. T. Pinho, "Plane contraction flows of upper convected Maxwell and Phan-Thien-Tanner fluids as predicted by a finite-volume method," J. Non-Newtonian Fluid Mech. **88**, 63–88 (1999).
[17]P. J. Oliveira and F. T. Pinho, "Numerical procedure for the computation of fluid flow with arbitrary stress-strain relationships," Numer. Heat Transfer, Part B **35**, 295–315 (1999).
[18]M. A. Alves, F. T. Pinho, and P. J. Oliveira, "The flow of viscoelastic fluids past a cylinder: Finite-volume high-resolution methods," J. Non-Newtonian Fluid Mech. **97**(2-3), 207–232 (2001).
[19]M. A. Alves, P. J. Oliveira, and F. T. Pinho, "A convergent and universally bounded interpolation scheme for the treatment of advection," Int. J. Numer. Methods Fluids **41**(1), 47–75 (2003).
[20]S. V. Patankar, *Numerical Heat Transfer and Fluid Flow* (Hemisphere Publishing Corporation, 1980).
[21]C. Rhie and W. Chow, "A numerical study of the turbulent flow past an isolated airfoil with trailing edge separation," AIAA J. **21**, 1525–1532 (1983).
[22]H. M. Matos, M. A. Alves, and P. J. Oliveira, "New formulation for stress calculation: Application to viscoelastic flow in a T-junction," Numer. Heat Transfer, Part B **56**(5), 351–371 (2010).
[23]J. Azaiez, R. Guénette, and A. Aitkadi, "Numerical simulation of viscoelastic flows through a planar contraction," J. Non-Newtonian Fluid Mech. **62**, 253–277 (1996).
[24]J. S. Lee, R. Dylla-Spears, N. P. Teclemariam, and S. J. Muller, "Microfluidic four-roll mill for all flow types," Appl. Phys. Lett. **90**, 074103 (2007).
[25]L. L. Ferrás, J. M. Nóbrega, and F. T. Pinho, "Analytical solutions for channel flows of Phan-Thien-Tanner and Giesekus fluids under slip," J. Non-Newtonian Fluid Mech. **171-172**, 97–105 (2012).
[26]D. O. A. Cruz, F. T. Pinho, and P. J. Oliveira, "Analytical solutions for fully developed laminar flow of some viscoelastic liquids with a Newtonian solvent contribution," J. Non-Newtonian Fluid Mech. **132**(1-3), 28–35 (2005).